Apoptosis (2020) 25:763–782
https://doi.org/10.1007/s10495-020-01633-1

Epoxyazadiradione exhibit activities in head and neck squamous cell carcinoma by targeting multiple pathways

Vipin Rai[1] · Sushil Kumar Aggarwal[2] · Sumit Singh Verma[1] · Nikee Awasthee[1] · Anupam Dhasmana[3,7] · Sadhna Aggarwal[4] · Satya N. Das[4,8] · Mangalam S. Nair[5] · Sanjay Yadav[6] · Subash C. Gupta[1]

Accepted: 30 August 2020 / Published online: 7 September 2020

Abstract

The head and neck squamous cell carcinoma (HNSCC) constitute about 90% of all head and neck cancers. HNSCC falls in the top 10 cancers in men globally. Epoxyazadiradione (EPA) and Azadiradione (AZA) are the limonoids derived from the medicinal plant *Azadirachta indica* (popularly known as Neem). Whether or not the limonoids exhibit activities against HNSCC and the associated mechanism remains elusive. Herein, we demonstrate that EPA exhibits stronger activity in HNSCC in comparison to AZA. The limonoids obeyed the Lipinski's rule of 5. EPA exhibited activities in a variety of HNSCC lines like suppression of the proliferation and the induction of apoptosis. The limonoid suppressed the level of proteins associated with anti-apoptosis (survivin, Bcl-2, Bcl-xL), proliferation (cyclin D1), and invasion (MMP-9). Further, the expression of proapoptotic Bax and caspase-9 cleavage was induced by the limonoid. Exposure of EPA induced reactive oxygen species (ROS) generation in the FaDu cells. N-acetyl-L-cysteine (ROS scavenger) abrogated the down-regulation of tumorigenic proteins caused by EPA exposure. EPA induced NOX-5 while suppressing the expression of programmed death-ligand 1 (PD-L1). Further, hydrogen peroxide induced NF-κB-p65 nuclear translocation and EPA inhibited the translocation. Finally, EPA modulated the expression of lncRNAs in HNSCC lines. Overall, these results have shown that EPA exhibit activities against HNSCC by targeting multiple cancer related signalling molecules. Currently, we are evaluating the efficacy of this molecule in mice models.

Keywords Carcinogenesis · Head and neck squamous cell carcinoma · Limonoid · Long non-coding RNA · Reactive oxygen species

Introduction

Head and neck cancer (HNC) is one of the ten common cancers globally. More than 650,000 cases are identified worldwide, out of which 330,000 dies of the disease annually [1]. HNC is a heterogeneous tumour at various anatomic sites

Electronic supplementary material The online version of this article (https://doi.org/10.1007/s10495-020-01633-1) contains supplementary material, which is available to authorized users.

✉ Subash C. Gupta
sgupta@bhu.ac.in

[1] Department of Biochemistry, Institute of Science, Banaras Hindu University, Varanasi 221005, India

[2] Department of Otorhinolaryngology, Institute of Medical Sciences, Banaras Hindu University, Varanasi 221 005, India

[3] Department of Biosciences, Himalayan Institute of Medical Sciences, Swami Rama Himalayan University, Jolly Grant, Dehradun 248 016, India

[4] Department of Biotechnology, All India Institute of Medical Sciences, Ansari Nagar, New Delhi 110029, India

[5] Division of Organic Chemistry, CSIR-National Institute for Interdisciplinary Science and Technology, Thiruvananthapuram, India

[6] Department of Biochemistry, All India Institute of Medical Sciences, Raebareli 229405, India

[7] Present Address: Department of Microbiology and Immunology, School of Medicine, University of Texas Rio Grande Valley, Edinburg, USA

[8] Present Address: Emeritus Scientist, Indian Council of Medical Research, Ansari Nagar, New Delhi, India

[2]. It accounts for one-fourth of male cancers and one-tenth of female cancers in India. HNC consistently metastasize to the cervical lymph nodes and the distant organs such as the liver and lung. Of all HNC, 90% is constituted by head and neck squamous cell carcinoma (HNSCC). Although people with over 60 years of age are prone to develop this disease, studies suggest that younger age group can also be affected by HNSCC [3, 4]. The hypopharynx, larynx, oropharynx, and oral cavity are the common locations for HNSCC [5]. Environmental and lifestyle factors such as tobacco chewing, alcohol consumption, and smoking are the main risk factors for HNSCC.

At the molecular level, multiple cancer related targets including the nuclear factor (NF)-κB contribute to the HNSCC pathogenesis [6]. The NF-κB signalling is also activated by epidermal growth factor receptor (EGFR) and PI3K pathways. In about 90% cases of HNSCC, EGFR is overexpressed [7]. The constitutively active NF-κB regulates cytokines production such as IL-6 and IL-8 in HNSCC [8]. Discovered in early 1980s, NF-κB has provided a link between inflammation and several human chronic diseases including cancer. Multiple cancer types including HNSCC constitutively express NF-κB. It is now well known that NF-κB regulates multiple cancer- related genes involved in tumour development [9]. Studies suggest that NF-κB cross talk with long non-coding RNAs (lncRNAs), the recently discovered class of non-coding RNAs [10]. Antisense non-coding RNA in the INK4 locus (ANRIL), NF-κB interacting lncRNAs (NKILA), Lethe, Metastasis Associated Lung Adenocarcinoma Transcript 1 (MALAT1), H19, and HOX transcript antisense RNA (HOTAIR) are some of the lncRNAs associated with the NF-κB signalling. The reactive oxygen species (ROS) are generated during normal conditions. ROS can also regulate various steps of tumour development [11]. ROS can contribute to tumour development through its cross talk with lncRNAs and NF-κB signalling [12].

The agents derived from Mother Nature are reported to be safe, affordable, and can modulate multiple cell signalling pathways. It is estimated that approximately 50% of the anticancer drugs (1940–2014) are directly or indirectly related to natural products [13]. *Azadirachta indica* (also called 'Neem' or 'nature's drugstore') is one such medicinal plant. The parts of this plant such as bark, flowers, leaves, and seeds are reported to possess activities against both acute and chronic human diseases. Over 300 structurally diverse constituents have been isolated from this plant, one-third of which are limonoids [14]. Two such limonoids are epoxyazadiradione (EPA) and azadiradione (AZA). Both EPA and AZA are reported to overcome Alzheimer's disease—associated Tau pathology [15]. AZA was found to produce strong cytotoxicity in HL60 leukemia cells with minimum effects on normal lymphocyte RPMI 1788 cell line [16]. In triple- negative and ER + breast cancer cells, EPA induced apoptosis and reduced mitochondrial potential, cell viability, angiogenesis, and migration [17]. Further, the expression of pro-metastatic and pro-angiogenic genes such as COX-2, VEGF, OPN, and MMP-9 was suppressed by the limonoid. EPA also attenuated AP-1 activation and suppressed tumour growth and angiogenesis in nude mice bearing breast cancer [17]. EPA was found to induce apoptosis and exhibit anti-cancer activities in cervical cancer cells with minimum effects in normal cells [18]. EPA also exhibited activities against neuroblastoma and osteosarcoma cells [19]. In RAW 264.7 cells, EPA inhibited proinflammatory activities [20]. EPA also inhibited the release of the cytokines (such as IL-1α, IL-6, IL-1β, and TNF-α) induced by LPS and migration inhibitory factor (MIF) in mice model. EPA was also found to prevent MIF-induced macrophage chemotactic migration, nuclear translocation of NF-κB, and nitric oxide production [20].

The implication of the above evidence suggests that EPA and AZA exhibit activities against some cancer types. Whether AZA and EPA exhibit activities against HNSCC and the underlying molecular mechanism is not known. In this study, we evaluated the activities and the associated mechanism of EPA and AZA in squamous cell carcinoma of the hypopharynx and the oral tongue.

Material and methods

Reagents

EPA and AZA were isolated from *Azadirachta indica* at the Council of Scientific and Industrial Research-National Institute for Interdisciplinary Science and Technology Thiruvananthapuram, India by the group of Dr. Mangalam Nair. We followed a method as described previously [18]. The reagents procured from Himedia (Mumbai, Maharashtra) were Dulbecco's modified Eagle's medium (DMEM), Trypsin–EDTA, streptomycin, and penicillin. The vendor for Dimethyl sulfoxide (DMSO), crystal violet, and 3-[4,5-dimethylthiazol-2-yl]-2,5-diphenyl tetrazolium bromide (MTT) was SRL Diagnostics (Mumbai, Maharashtra). Acridine orange, propidium iodide, ethidium bromide, 4′,6-diamidino-2-phenylindole (DAPI), agarose, 5, 5′, 6, 6′-Tetrachloro-1, 1′, 3, 3′-tetraethyl benzimidazolyl carbocyanineiodide (JC-1), fetal bovine serum (FBS), 2′,7′-dichlorodihydrofluorescein diacetate (H_2DCFDA), Alexa Fluor 488, and Annexin V staining kit were purchased from Invitrogen (Carlsbad, California). Antibodies against Bcl-xL, Bcl-2, and survivin were procured from Santa Cruz Biotechnology (Santa Cruz, California), and the p65 antibody was obtained from Abcam (Cambridge, UK). PDL-1 antibody was obtained from proteintech (Rosemont, Illinios). The mouse NOX-5 antibody was a gift from Dr. Smitha Antony,

National Cancer Institute, National Institutes of Health, USA. The SYBR green PCR master mix was purchased from Agilent Technologies (Foster City, California). The primers for Cyclin D1, Bcl-2, ANRIL, MALAT1, MEG3, H19, HOTAIR, GAS5, and GAPDH were synthesized by Eurofins Genomics (Bangalore, Karnataka).

Cell lines

The human head and neck cancer cell lines, FaDu, SCC-4 and Cal-27 (American Type Culture Collection; Manassas, VA) were obtained from the laboratories of Dr. Sanjay Yadav and Dr. Satya N. Das. The cell lines were cultured in the DMEM (high glucose) containing streptomycin (100 µg/mL), penicillin (100 units/mL), and FBS (10%).

Assay for cell viability

The MTT substrate- based assay was employed for determining the cytotoxic potential of EPA and AZA in HNSCC [21]. In brief, the viability in control and treated cells was determined by estimating the mitochondrial reductase activity and measuring the absorbance of the purple formazan formed at 570 nm.

Colony formation assay

Colony formation assay was used to determine the ability of cells to grow into colonies as described in an earlier study [22]. The cells (1000/well) were cultured for 6 h in the absence or presence of various concentrations of EPA. The cells were washed to remove EPA and the colony formation was monitored for 10 days. The counting of the colonies was performed in a manual manner after staining with 0.25% crystal violet.

DAPI staining

This staining was used to examine if EPA affects the nuclear morphology [23]. After exposing to the different concentrations of EPA, the cells were washed with PBS. Then, 4% paraformaldehyde was used for fixation for 15 min at room temperature. After permeabilization with methanol, the cells were stained with DAPI at room temperature. Finally, the cells were visualized under the fluorescence microscope to determine the changes in the nuclear morphology.

Acridine orange/propidium iodide (AO/PI) staining

We used AO/PI staining to determine the effects of EPA on the morphology of cells. The healthy cells with intact membrane produce green fluorescence. The characteristics such as membrane blebbing and nuclear condensation are observed when the cells are in the early phases of apoptosis. Briefly, the normal and treated cells were stained with AO/PI (100 µg/mL) and visualized under the fluorescence microscope.

DNA fragmentation assay

DNA laddering is the characteristic of the late stages of apoptosis. For this assay, we employed a method described previously [24]. The cells were lysed in lysis buffer containing Tris (100 mM-pH 8.0), EDTA (20 mM), RNaseA (500 unit/mL), and SDS (0.8%) at 37 °C for 30 min. The lysate was then deproteinized using proteinase K (20 mg/mL) at 55 °C for 2 h. Chloroform and isopropanol were used for the DNA precipitation. We used 70% ethanol to wash the precipitate before air drying. The DNA was dissolved in Tris–EDTA buffer and electrophoresed over agarose gel (1.5%). Finally, the DNA was visualized and imaged using the BioRad Gel Doc XR + documentation system.

Cell cycle analysis

Whether EPA affects cell cycle phases was evaluated by PI staining [25]. The control and treated cells were washed with PBS and fixed with chilled methanol (70%) before treatment with RNaseA. PI was used to stain the cells and assessment was performed by flow cytometer. The population in different phases of the cell cycle was analysed by cell quest software (Becton Dickinson).

Evaluation of mitochondrial membrane potential (ΔΨ)

We used the fluorochrome, JC-1 to evaluate the depolarization in mitochondrial membrane potential [26]. Briefly, the normal and exposed cells were washed and stained with 10 µM JC-1 in the dark at 37 °C for 20 min. The stained cells were analysed by flow cytometry. While intact mitochondria produce red fluorescence, the cells with depolarized mitochondria produce green fluorescence. The FL1-H indicates green fluorescence, while FL2-H represents the red fluorescence.

Assay for cellular localization of p65

Whether EPA affects the cellular localization of p65 was evaluated by immunocytochemistry [27]. Hydrogen peroxide (H_2O_2) was used to induce nuclear translocation of p65. The FaDu cells were treated with EPA before stimulation with H_2O_2. The cells were then incubated with rabbit p65 antibody followed by Alexa Fluor 488 conjugated anti-rabbit secondary antibody. After counterstaining with DAPI,

cells were visualized and imaged under the fluorescence microscope.

Western blotting

To examine the expression pattern of tumorigenic proteins, we performed western blotting [28]. The whole cell extract was prepared from the normal and exposed cells and resolved by SDS-PAGE. The electrophoresed protein was then transferred onto nitrocellulose membrane and probed with primary and secondary antibodies. Finally, the signals were detected by using ECL reagent.

Scratch assay

We performed scratch assay to examine the effects of EPA on cell migration [29]. The FaDu cells were allowed to grow till 80% confluency. The cell monolayer was then wounded using a sterile tip. The debris was then washed off and the cells were cultured in the absence or presence of EPA. We used phase contrast microscope to examine the width of the wounded area at 0, 12 and 24 h of EPA treatment. At each time point, we calculated the percentage of the healed area and wound size using the Image J software.

Semi-quantitative and quantitative RT-PCR

We examined the effects of EPA on the expression of Bcl-2 and cyclin D1 by the semiquantitative RT-PCR analysis. The quantitative real-time PCR analysis was carried out to examine if EPA modulates the expression of lncRNAs [30].

Table 1 provides a list of the primer sequences of the genes of interest. The Trizol reagent was used for the extraction of the total RNA from the control and exposed cells. The high capacity cDNA synthesis kit (Invitrogen) was used for the reverse transcription of RNA. The PCR product was electrophoresed over the agarose gel (1.5%). The image Lab™ software was used for the densitometric quantification of the DNA bands. GAPDH was used for the normalization of the data. The lncRNAs expression pattern was analysed by the quantitative real-time PCR analysis. The fold change in the lncRNAs expression pattern was quantified by $2^{-\Delta\Delta CT}$ method [31]. The normalization of the quantitative RT-PCR data was performed using the house-keeping genes (5S rRNA and ACTB).

Computational analyses

Drug like properties of EPA (PubChem ID: 49863985) and AZA (PubChem ID: 12308714) were examined using the Lipinski's rule of 5 (https://www.molinspiration.com//cgi-bin/properties). The screening for Absorption, Distribution, Metabolism, Excretion & Toxicity (ADMET) was also carried out as described earlier [32]. The putative bioactivity was evaluated from the additional feature of molinspiration. PubChem database was used for the SMILE IDs of EPA and AZA. The SMILE IDs were converted to *.pdb* files using CORINA 3D server. RCSB protein databank was used to download crystal structures of NF-κB-p65 (1NFI Chain A), NF-κB-p50 (1NFI Chain B) and IκBα (Chain E). IKKα and TAK-1 were procured from 5TQY and 2EVA, respectively. The binding affinities and binding pattern of proteins and ligands were predicted using the MGL tool [33, 34].

Statistical analysis

The two groups i.e., treatment and control were compared using the unpaired Student's *t*-test. The significance level was ascribed at a value of $P < 0.05$.

Table 1 The sequences of the primers used in the semi-quantitative and quantitative RT-PCR

Gene/lncRNA	Forward sequence (5′–3′)	Reverse sequence (5′–3′)
Semi-quantitative RT-PCR		
Bcl-2	GGGTATGAAGGACCTGTATTGG	CATGCTGATGTCTCTGGAATCT
Cyclin D1	CTCCACCTCACCCCCTAAAT	AGAGCCCAAAAGCCATCC
GAPDH	GCTCTCTGCTCCTCCTGTTC	ACGACCAAATCCGTTGACTC
Quantitative RT-PCR		
H19	ATCGGTGCCTCAGCGTTCGG	CTGTCCTCGCCGTCACACCG
GAS5	CTTCTGGGCTCAAGTGATCCT	TTGTGCCATGAGACTCCATCAG
MEG3	CTGCCCATCTACACCTCACG	CTCTCCGCCGTCTGCGCTAGGGGCT
ANRIL	TGCTCTATCCGCCAATCAGG	GGGCCTCAGTGGCACATACC
HOTAIR	GGTAGAAAAAGCAACCACGAAGC	ACATAAACCTCTGTCTGTGAGTGCC
MALAT1	TGATAGCCAAATTGAGACAA	TTCAGGGTGAGGAAGTAAAA
ACTB	CTGTGGCATCCACGAAAC	CAGACAGCACTGTGTTGG
5S rRNA	GGCCATACCACCCTGAACGC	CAGCACCCGGTATTCCCAGG

Results

The goal of this study was to determine the comparative efficacy of EPA and AZA in HNSCC. Although most of the experiments were performed using EPA, preliminary experiments were performed using AZA as well. We used the cell lines from the squamous cell carcinoma of the hypopharynx (FaDu) and the oral tongue (SCC4, Cal-27). The mechanism for the activities of EPA in HNSCC was also examined.

NF-κB activation is suppressed by EPA in HNSCC

Because NF-κB regulates the expression of tumorigenic proteins, we examined whether EPA can suppress NF-κB activation in HNSCC. Under control conditions, the p65 subunit of NF-κB is located mostly in the cytoplasm. In response to the inducing stimuli, p65 translocate from cytoplasm to the nucleus. We used H_2O_2 for the activation of NF-κB before treatment with EPA. The microenvironment of tumours is characterized by high concentration of H_2O_2 that acts as a double-edged sword [35]. While H_2O_2 induced nuclear accumulation of p65, EPA alone was unable to affect NF-κB activation (Fig. 1a). However, when FaDu cells were treated with EPA before stimulation with H_2O_2, p65 nuclear accumulation was drastically reduced.

We also employed molecular docking tools to examine if EPA and AZA can interact with the regulatory molecules in the NF-κB signalling. The dissociation constant (Ki, μM) and binding energies (kcal/mol) values of NF-κB p65, NF-κB p50, inhibitor of kappa-B alpha (IκBα), IκB kinase alpha (IKKα), and transforming growth factor-β-activating kinase-1 (TAK1) with EPA were 88.26 and − 5.53, 29.55 and − 6.18, 3.75 mM and − 3.31, 13.75 and − 6.63, 17.77 and − 6.48, respectively (Table 2; Fig. 1b). Similarly, the Ki (μM) and binding energies (kcal/mol) values of IκBα, NF-κB p50, NF-κB p65, TAK1, and IKKα with AZA were 631.27 and − 4.37, 11.80 and − 6.72, 14.70 and − 6.59, 5.81 and − 7.14, 23.60 and − 6.31, respectively (Table 2; Fig. 1c). The affinity of IκBα, p50, p65, and TAK1 was slightly higher for AZA as compared to EPA. However, IKKα exhibited a higher affinity for EPA as compared to AZA.

The lncRNAs expression is modulated by EPA in HNSCC

The lncRNAs are the recently emerged class of non-coding RNAs with an ability to modulate the process of tumorigenesis. The lncRNAs cross talk with cancer related signalling molecules including NF-κB. We observed that EPA modulated the expression of lncRNAs in HNSCC lines. When SCC-4 cells were exposed to 10–25 μM EPA, the expression of ANRIL, MALAT1, MEG3, H19, and HOTAIR was suppressed (Fig. 2a). For example, the expression of MALAT1 was reduced to 0.43-folds and 0.33-folds in SCC-4 cells by 10 μM and 25 μM EPA, respectively. Similarly, the expression of H19 was reduced to 0.18-folds and 0.14-folds in SCC-4 cells by 10 μM and 25 μM EPA, respectively. However, the expression of GAS-5 and HOTAIR was enhanced by EPA in FaDu cells (Fig. 2b). Collectively, EPA can modulate the lncRNAs expression in HNSCC.

EPA induces ROS generation and NOX-5 in HNSCC

Next, we examined if EPA can induce ROS generation in HNSCC lines. FaDu cells were exposed for 1 h with 1–25 μM EPA and ROS generation was estimated by flow cytometry. EPA induced ROS in HNSCC in a dose- dependent manner. For example, ROS generation was increased by 2.3-folds and 2.8-folds by 10 μM and 25 μM EPA, respectively (Fig. 2c). The ROS is produced inside the cell through multiple mechanisms, the major of which is through the involvement of NADPH oxidase (NOX) complex in cell membranes [36]. NOX exists in multiple forms, one of which is NOX-5. We examined if EPA can induce NOX-5 expression. Cells were treated with 25 μM EPA from 30 min to 24 h. The whole cell extract was used for NOX-5 expression by western blotting. The NOX-5 expression was induced by EPA in a time-dependent manner (Fig. 2d). For example, 1.2-folds and 1.5-folds induction in the expression was observed after 6 h and 24 h, respectively.

EPA modulates the expression of tumorigenic proteins in HNSCC

Because EPA suppressed the NF-κB activation, we evaluated its effect on the expression of tumorigenic proteins. FaDu cells were exposed to 1–25 μM EPA for 24 h. The whole cell extract was then used for the expression of proteins. The cell survival proteins such as Bcl-xL, Bcl-2, and survivin were suppressed by EPA (Fig. 3a). For example, the level of Bcl-xL was reduced to 0.49-folds and 0.42-folds at 5 μM and 25 μM EPA, respectively. Similarly, the level of survivin was suppressed to 0.95-folds and 0.01-folds at 5 μM and 25 μM EPA, respectively. The level of MMP-9, which is involved in tumour invasion was also suppressed by EPA. Conversely, EPA induced the expression of Bax (pro-apoptotic protein) and caspase-9 cleavage in HNSCC line. For example, the level of cleaved caspase-9 was increased by 1.87-folds at 25 μM EPA. Programmed death-ligand 1 (PD-L1), a transmembrane protein is an immunosuppressive molecule. Cancer cells evade the immune response due to higher expression of PD-L1 [37]. EPA was found to suppress PD-L1 expression in HNSCC cell line. We also observed

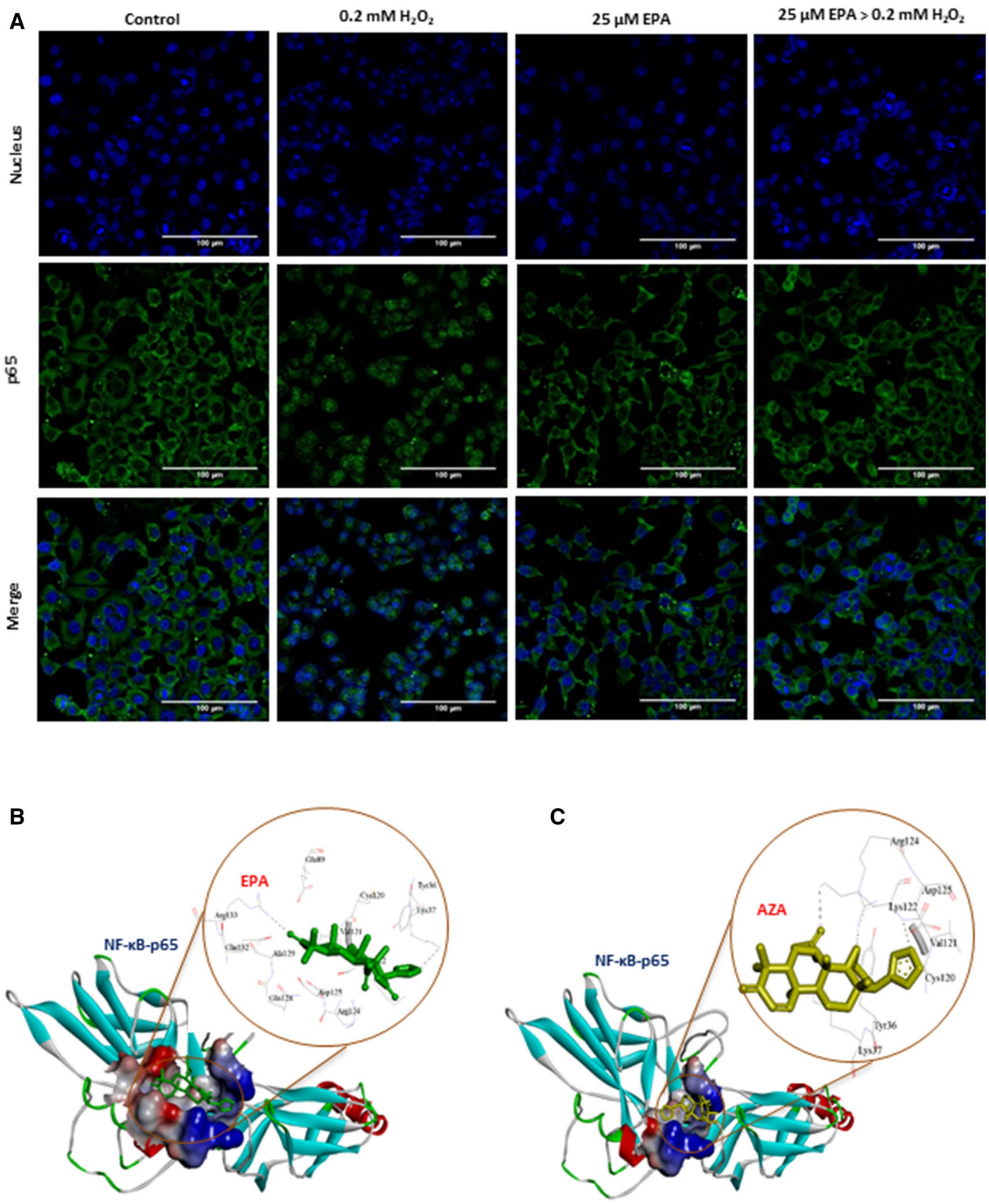

Fig. 1 EPA reduces NF-κB activation in HNSCC lines and binds with p65 subunit of NF-κB. **a** FaDu cells were exposed to 25 µM EPA for 6 h. Then, the cells were stimulated with 0.2 mM H_2O_2 for 1 h. The content of p65 in the cytoplasm and nucleus was then determined by immunocytochemistry. Note a reduction in the H_2O_2 induced nuclear accumulation of p65 after EPA treatment. **b**, **c** The binding interaction analysis and binding pose of EPA and AZA with NF-κB p65. *AZA* azadiradione; *EPA* epoxyazadiradione

Table 2 Molecular docking analyses of EPA and AZA with key proteins of NF-κB signalling pathway

Receptor	Ligand: EPA		Ligand: AZA	
	Binding energy (kcal/mol)	Ki (μM)	Binding energy (kcal/mol)	Ki (μM)
IκBα	− 3.31	3.75 mM	− 4.37	631.27
NF-κB-p50	− 6.18	29.55	− 6.72	11.80
NF-κB-p65	− 5.53	88.26	− 6.59	14.70
TAK1	− 6.48	17.77	− 7.14	5.81
IKKα	− 6.63	13.75	− 6.31	23.60

AZA azadiradione; *EPA* epoxyazadiradione

that EPA can suppress the mRNA transcript of Cyclin D1 and Bcl-2 (Fig. 3b).

Whether the modulation in the expression of tumorigenic proteins by EPA is mediated through ROS was examined. We used N-acetylcysteine (NAC), the ROS scavenger to examine this possibility. FaDu cells were exposed to 1–10 mM NAC before treatment with 25 μM EPA. While EPA reduced the expression of MMP-9, Bcl-2, and Bcl-xL, NAC alone was unable to modulate the expression of these proteins (Fig. 3c). When FaDu cells were exposed with NAC before EPA, the suppression in the expression of Bcl-2, MMP-9, and Bcl-xL was almost completely reversed. Overall, it can be concluded that the suppression in the expression of Bcl-xL, Bcl-2, and MMP-9 by EPA is mediated through ROS.

EPA exhibit anti-proliferative activities and reduces colony formation in HNSCC lines

Because EPA modulated the expression of tumorigenic proteins, we evaluated if this limonoid can reduce the proliferation of HNSCC lines. FaDu cells were exposed to 0.1 μM to 100 μM EPA for 24 h to 72 h and the viability was determined by estimating the mitochondrial reductase activity. We also compared the anti-proliferative activities of EPA with AZA, which is another limonoid. Both EPA and AZA exhibited antiproliferative activities in a concentration and time- dependent manner (Fig. 4b). However, EPA exhibited stronger activities in comparison to AZA (Fig. 4c). For example, the viability was reduced by 72.8% and 79.3%, when FaDu cells were treated for 72 h with 25 μM and 50 μM EPA, respectively. However, the proliferation was suppressed by 58.4% and 65.2%, when FaDu cells were treated for 72 h with 25 μM and 50 μM AZA, respectively. The cell proliferation (percent of control) was drawn over concentration (log) μM of EPA and AZA in FaDu cells at 24, 48 and 72 h and IC_{50} value was calculated using GraphPad Prism software. The IC_{50} value for EPA was found to be 16.2 μM, 8.3 μM and 1.6 μM after 24 h, 48 h and 72 h, respectively (Fig. S1*A*). However, IC_{50} value for AZA was observed at 39.9 μM, 15.4 μM and 8.4 μM after 24 h, 48 h and 72 h, respectively (Fig. S1*B*). Overall, these results suggest that EPA exhibit stronger anti-proliferative activities in comparison to AZA.

We also examined the drug- like properties of EPA and AZA using Lipinski's rule of 5 (Table 3). The values for lipophilicity (log P: 3.66 for EPA and 4.23 for AZA), topological polar surface area (TPSA: 86.11 for EPA and 73.59 for AZA), molecular weight (466.57 for EPA and 450.57 for AZA), hydrogen bond acceptor (6 for EPA and 5 for AZA), hydrogen bond donor (0 for EPA and 0 for AZA), and rotatable bonds (3 for EPA and 3 for AZA) suggested that both EPA and AZA obeyed Lipinski's rule of 5 (Table 3). Next, we predicted the bioactivity (Table 4; Fig. 4d) and performed ADMET analysis (Table 5) for EPA and AZA. Both the limonoids exhibited almost similar characteristics. For example, strong nuclear receptor ligand and enzyme inhibitor activity was observed by both EPA and AZA (Table 4; Fig. 4D). The two limonoids also exhibited slight GPCR ligand and ion channel modulator activities. Unlike AZA, EPA exhibited protease inhibitor activity. The kinase inhibitor activity was not observed by any of these limonoids. From the ADMET analysis, we observed that both EPA and AZA can cross the blood-brain barrier and intestine (Table 5). Further, both limonoids did not exhibit any evidence of carcinogenicity and genotoxicity (Table 5). Overall, these observations suggest that EPA and AZA possess drug- like properties.

Whether the effects of EPA are restricted to FaDu cells or it exhibits activities in other HNSCC lines was examined. EPA suppressed the proliferation of squamous cell carcinoma of the oral tongue such as Cal-27 and SCC-4 in a dose- (Fig. 5a) and time-dependent manner (Fig. 5b). However, Cal-27 cells were sensitive to EPA as compared to SCC-4. For example, the proliferation of Cal-27 cells was suppressed by 55.6% at 25 μM EPA after 72 h. On the other hand, the proliferation of SCC-4 cells was suppressed by 36.8% at 25 μM EPA after 72 h. Further, the IC_{50} value of EPA in Cal-27 cells was observed at 17.69 μM, 11.52 μM and 5.7 μM after 24 h, 48 h and 72 h, respectively (Fig. S2*A*). The IC_{50} value was observed at 80.0 μM, 64.4 μM and 26.9 μM after 24 h, 48 h and 72 h, respectively in SCC-4 cells (Fig. S2*B*). These observations further confirmed stronger sensitivity of Cal-27 to EPA in comparison to SCC-4.

Next, we examined if EPA can affect the long-term colony formation of HNSCC lines. The colony formation is a characteristic of tumour cells and mimics the in-vivo situation. The FaDu cells were exposed to 1–25 μM EPA for 24 h. The EPA was removed by washing and the colony formation was monitored for 10 days. EPA reduced the colony formation in a dose-dependent manner (Fig. 5c). The colony formation

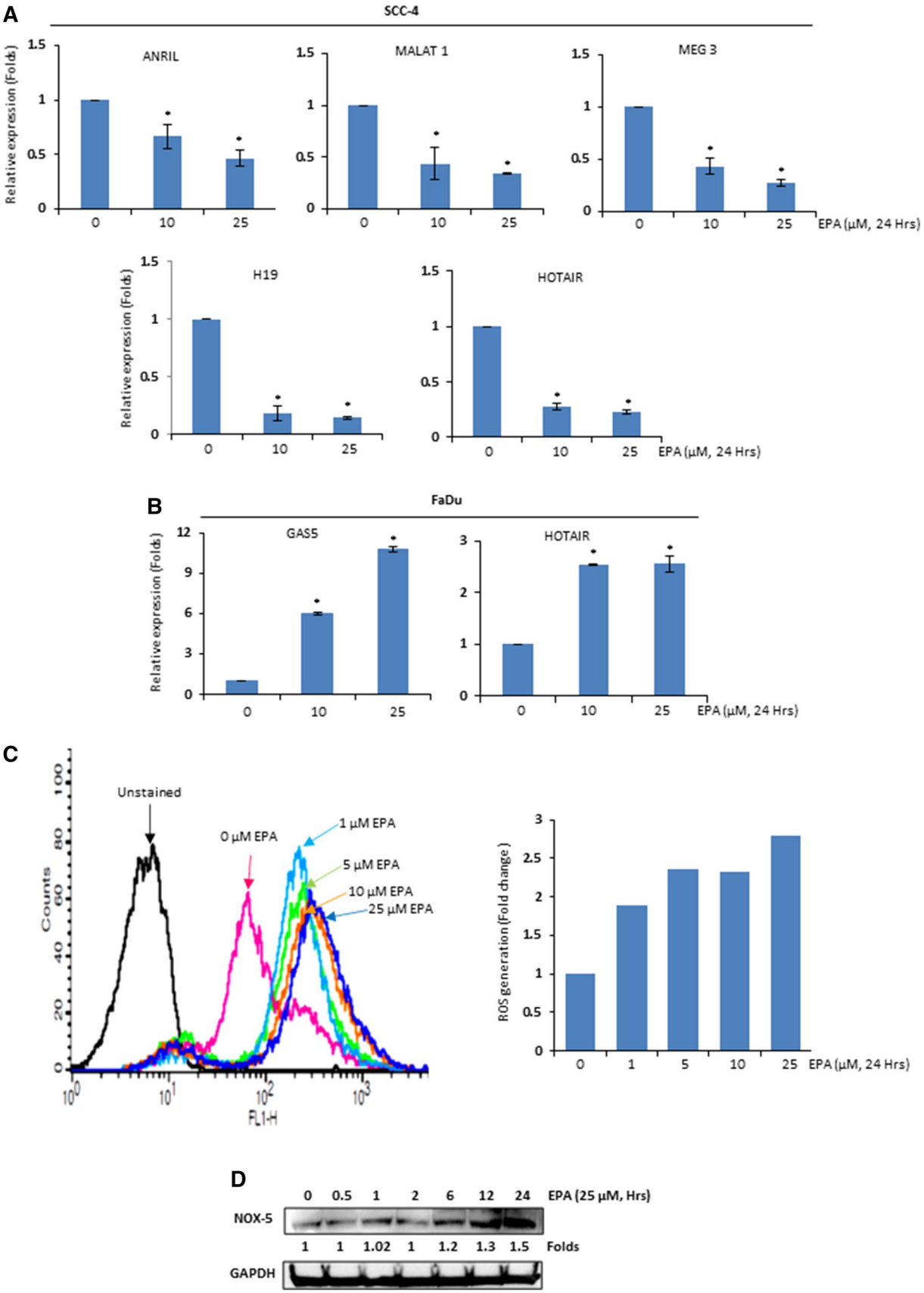
A
SCC-4
ANRIL
MALAT 1
MEG 3
H19
HOTAIR
Relative expression (Folds)
EPA (μM, 24 Hrs)
B
FaDu
GAS5
HOTAIR
C
Unstained
0 μM EPA
1 μM EPA
5 μM EPA
10 μM EPA
25 μM EPA
Counts
FL1-H
ROS generation (Fold change)
D
EPA (25 μM, Hrs)
NOX-5
GAPDH
Folds

◂**Fig. 2** EPA modulates the expression of lncRNAs, NOX-5, and induces ROS generation in HNSCC lines. **a**, **b** SCC-4 and FaDu cell lines were treated for 24 h with 10–25 μM EPA. TRIZOL reagent was used for RNA extraction. RNA was then reverse transcribed and analysed for lncRNAs expression by quantitative RT-PCR. **c** The FaDu cells were exposed to indicated concentrations of EPA. After 1 h, the cells were incubated for 30 min with H_2DCFDA. The ROS generation was estimated by flow cytometry. **d** Cells were treated with 25 μM EPA from 30 min to 24 h. Whole cell extract was used for NOX-5 expression by western blotting. Where indicated, values are average ± SE from 3 experiments. The significance level (*) was determined in comparison to the control group; $P < 0.05$. *EPA* epoxyazadiradione

was reduced by 12.5%, 34.7%, and 54.5% by 1 μM, 10 μM and 25 μM EPA, respectively. Collectively, EPA suppresses the colony formation by FaDu cells that may be applicable to other HNSCC lines.

EPA induces apoptosis in HNSCC lines through the mediation of mitochondria

One strategy of cancer treatment is to trigger death in tumour cells in a designed manner (apoptosis) without affecting normal cells. Whether EPA induces apoptosis in HNSCC lines was examined by a number of assays. We examined the cell viability after EPA treatment by AO/PI staining assay. Because of its permeability to both live and dead cells, AO stains the nucleated cells and produces green fluorescence. On the other hand, only the dead cells with reduced membrane integrity are stained with PI. The dead nucleated cells produce red fluorescence after staining with PI. We observed a reduction in the viability of FaDu cells after increasing the concentration of EPA (Fig. 6a). The characteristics of apoptosis such as nuclear condensation and membrane blebbing were observed after treatment with EPA. We measured the cell population in different phases of the cell cycle after staining with PI. The subG1 population was increased by increasing EPA concentration. For instance, the subG1 population was observed at 1.75% and 7.84% by 5 μM and 25 μM EPA, respectively (Fig. 6b).

The early phase of apoptosis is characterized by the phosphatidylserine (PS) externalization on the outer surface of the plasma membrane. Due to the affinity with the PS, Annexin V can be used to analyse the population of early apoptotic cells. In the control FaDu cells, no early apoptotic cells were observed. However, treatment of cells was associated with an increase in the number of early apoptotic cells (Fig. 6c). For instance, the early apoptotic cells were observed at 28.83% and 38.16% by 5 μM and 25 μM EPA, respectively.

The advanced stages of apoptosis are associated with the DNA cleavage (180–200 base pairs) in the form of ladders. We observed DNA smearing pattern in the FaDu cells exposed with 10 μM and 25 μM EPA (Fig. 6d). However, in the control and in the cells treated with lower concentrations of EPA, DNA was intact. The changes in the nuclear morphology of normal and treated cells were also examined after DAPI staining. While normal cells exhibited round or oval- shaped (normal) nuclei, chromatin condensation and nuclear fragmentation were observed in EPA treated cells (Fig. 6e).

Whether EPA induced apoptosis in HNSCC lines is mediated through mitochondria was investigated. For this, we used JC-1 fluorochrome. The healthy and depolarized mitochondria were examined by measuring changes in MMP using JC-1 dye. In normal cells, JC-1 exists as aggregates (red, upper right quadrant) and indicate normal MMP. In cells with depolarized mitochondria, JC-1 exists as monomers (green, lower right quadrant). In control cells, JC-1 was observed as aggregates (Fig. 6f). With an increase in EPA concentration, a reduction in JC-1 aggregates and an induction in JC-1 monomer was observed (Fig. 6f). For example, the red/green ratio (healthy/depolarized mitochondria) was observed at 17.61 in the control cells. However, the ratio was observed at 5.72 in the group of cells treated with 25 μM EPA (Fig. 6g).

EPA suppresses the migration of HNSCC

One feature of HNSCC is its metastasis to cervical lymph nodes, liver, and lung. The metastasis is preceded by migration and invasion. Whether EPA affects the migration of FaDu cells was examined by wound healing scratch assay (Fig. 7a). The control FaDu cells exhibited a respective 36.9% and 27.6% of the original wound area after 12 h and 24 h (Fig. 7b). EPA was found to significantly reduce the wound areas. At 1 μM EPA, the wound area was observed at 42% and 36.6% after 12 h and 24 h, respectively (Fig. 7b). Similarly, at 5 μM EPA, the wound area was observed at 57% and 52.3% after 12 h and 24 h, respectively (Fig. 7b). In the control group, the healing was observed at 63% and 72.3% after 12 h and 24 h, respectively (Fig. 7c). The healed area was reduced with an increase in EPA concentration (Fig. 7c). Collectively, EPA can suppress the migration of FaDu cells.

Discussion

HNSCC is an epithelial malignancy that originates from the mucosal lining of hypopharynx, larynx, oral cavity, and oropharynx. Studies suggest that the rate of HNSCC occurrence is more than twice in men as compared to women [5]. The causative factors for HNSCC include tobacco-chewing, betel or areca nut chewing, and cigarette-smoking [5]. Although chemotherapy, radiotherapy, and surgery are used as the standard treatment for HNSCC, the survival rate has not improved over the years. Approximately 30–50% of HNSCC

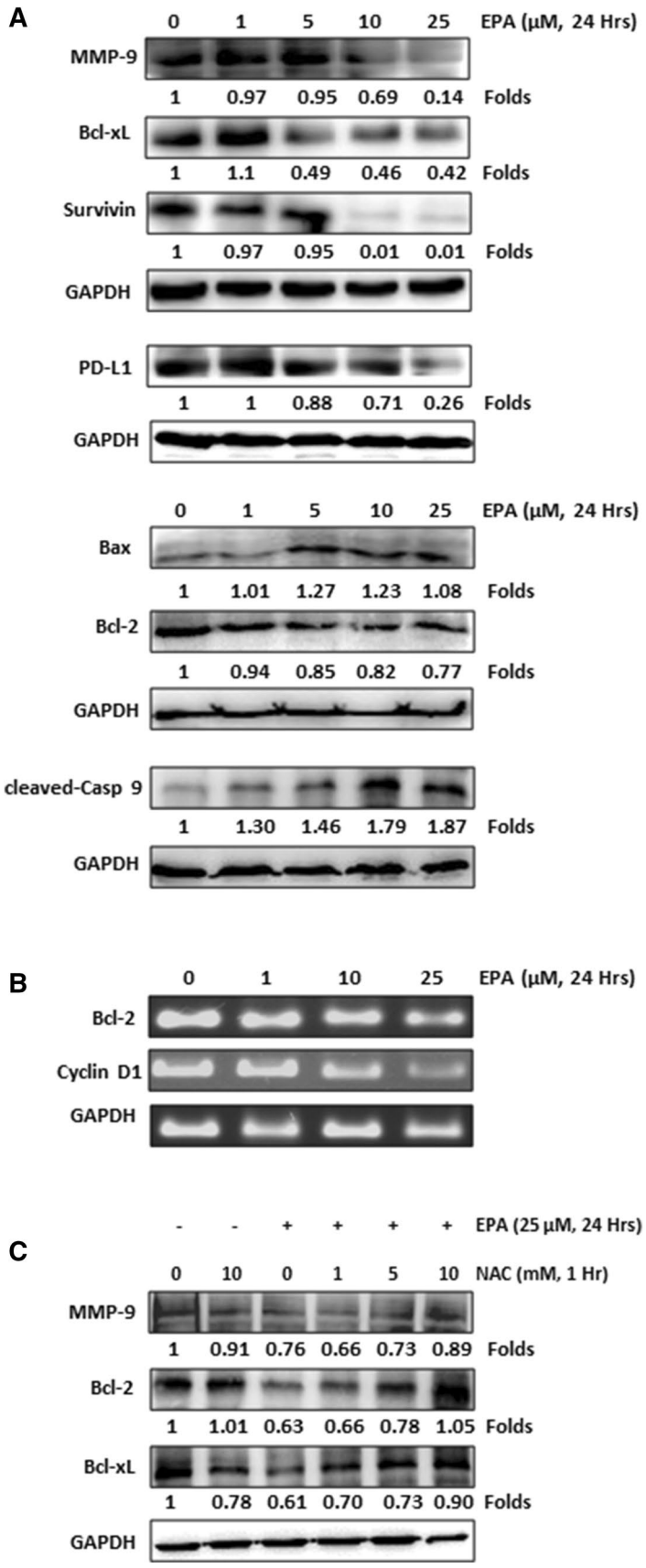

Fig. 3 EPA modulates the tumorigenic proteins in HNSCC lines. **a** FaDu cells were treated with 1–25 μM EPA for 24 h. The whole cell extract was used to evaluate the expression of indicated proteins by western blotting. GAPDH was used for the normalization of the data. **b** The RNA was isolated from the normal and EPA treated cells and reverse transcribed. The cDNA was amplified by PCR, electrophoresed, and stained with ethidium bromide. GAPDH was used for the normalization of the data. **c** FaDu cells were treated with NAC before EPA and the indicated proteins were evaluated by western blotting. GAPDH was used for the normalization of the data. *EPA* epoxyazadiradione

patients are estimated to develop a regional or local recurrence [38]. Further, many patients develop metastases to distant organs [38]. Therefore, novel therapeutics with better efficacy and minimum side effects are required.

It is now well documented that the dysregulation in several genes contributes to the pathogenesis of multiple cancer types including HNSCC. Yet, majority of the chemotherapeutics are designed based on a single target. We determined the efficacy of EPA and AZA in a number of HNSCC lines such as FaDu, SCC4, and Cal-27 in this study. Both EPA and AZA are limonoids derived from *Azadirachta indica* (Neem). The parts of this plant have been used since ancient times to treat human ailments [14]. We observed that H_2O_2 induced p65 nuclear translocation in HNSCC and EPA suppressed the translocation. The pro-inflammatory role of NF-κB is now well established. As many as 500 cancer -related genes are regulated by this transcription factor [39]. We also observed that the proteins involved in anti-apoptosis such as Bcl-xL, Bcl-2, and survivin were downregulated while pro-apoptotic Bax was upregulated. Because NF-κB regulates the expression of these proteins [40], a possibility that suppression in the expression of these proteins by EPA is due to its negative effects on NF-κB cannot be ruled out. These observations also suggested that EPA induces apoptosis in HNSCC. In fact, assays such as AO/PI staining, DAPI staining, and DNA fragmentation suggested the potential of EPA in triggering apoptosis at the molecular and cellular levels. The observations that EPA induces caspase-9 cleavage suggest the role of mitochondria in the apoptosis induction by this limonoid. The involvement of mitochondria in the EPA induced apoptosis was further confirmed by the disruption in the mitochondrial membrane potential. Consistent with these observations, EPA is known to induce apoptosis in triple- negative breast cancer [17], ER + breast cancer [17] and cervical cancer [18]. The major cause of death due to HNSCC is not the primary tumour but because of the metastasis to the distant organs [41]. We observed that EPA suppresses HNSCC migration which is a step before invasion and metastasis. Because of its ability to suppress MMP-9 expression, the limonoid may also reduce the invasion activity of HNSCC. In agreement with these observations, EPA was also found to suppress migration in triple-negative and ER + breast cancer cells [17].

The cross-talk of NF-κB with other signalling molecules and transcription factors is well documented [42]. NF-κB has also been reported to cross talk with lncRNAs [10]. A dysregulation in the HOTAIR expression is reported in several cancer types [43]. In ovarian cancer cells, the upregulation in the HOTAIR expression associate with an enhancement in NF-κB activation [44]. Conversely, LPS induced HOTAIR significantly suppressed NF-κB activation in chondrocytes and in a mouse model of rheumatoid arthritis [30]. In our observations, EPA induced HOTAIR expression in FaDu cells. However, HOTAIR expression was suppressed in SCC-4 cells by EPA. Similar to these observations, paclitaxel was found to suppress HOTAIR expression in laryngeal squamous cell carcinoma [45]. Overall, the limonoid modulates the expression of HOTAIR in HNSCC in a cell type-specific manner. It is possible that EPA induced HOTAIR to abrogate NF-κB activation in FaDu cells. Whether EPA modulates NF-κB activation in SCC-4 cells remain to be investigated. EPA was also found to induce GAS5 in FaDu cells. The tumour suppressor function of GAS5 is reported in multiple cancer types [46]. The suppressed expression of GAS5 could promote tumorigenic properties in esophageal squamous cell carcinoma [47]. Further, GAS5 can predict the response of head and neck cancer patients to therapy [48]. It is likely that the induced expression of GAS5 in response to EPA contributes to its anti-carcinogenic activities. The GAS5 expression is significantly enhanced during the growth arrest of the tumour cells [49]. In agreement with this report, we observed an enhancement in the subG1 population of FaDu cells with an increase in the EPA concentration. Our unpublished observations indicate that the anti-proliferative activities of EPA are abrogated by the gene silencing of GAS5. This suggests that GAS5 is required for the anti-proliferative activities of EPA.

ROS generated during normal conditions is also known to regulate multiple aspects of tumour development [11]. Moreover, the interaction between ROS and lncRNAs can control the process of tumorigenesis [12]. In our observations, EPA induced ROS generation in HNSCC lines. The EPA induced suppression in the expression of Bcl-xL, Bcl-2, and MMP-9 were reversed by the use of NAC, which is a ROS scavenger. These observations suggest that EPA reduces the expression of these proteins through the generation of ROS. In agreement with these observations, a chalcone exhibited activities in colon cancer cells through ROS generation [50]. Similarly, licochalcone C induced apoptosis in human esophageal squamous carcinoma cells through ROS generation [51]. An induction in NOX-5 expression suggests that this oxidase might be required for ROS generation in response to EPA in HNSCC lines. In agreement with these observations, an increase in the activity and expression of NOX-5 was reported in multiple cancer types [52].

Both EPA and AZA obeyed the 'five rules of Lipinski' suggesting their drug- like properties. The limonoids exhibited the permeability to the blood-brain barrier and intestinal absorption. The inability of EPA and AZA to exhibit carcinogenic and genotoxic properties further confirmed their drug- like properties. However, EPA was more effective in comparison to AZA. Whereas EPA contains 3-membered epoxy ring, AZA has a double bond. Whether the epoxy ring is responsible for the stronger anti-cancer activity of EPA remains to be elucidated. Previous studies have demonstrated that EPA possesses insecticidal [53] and anti-malarial

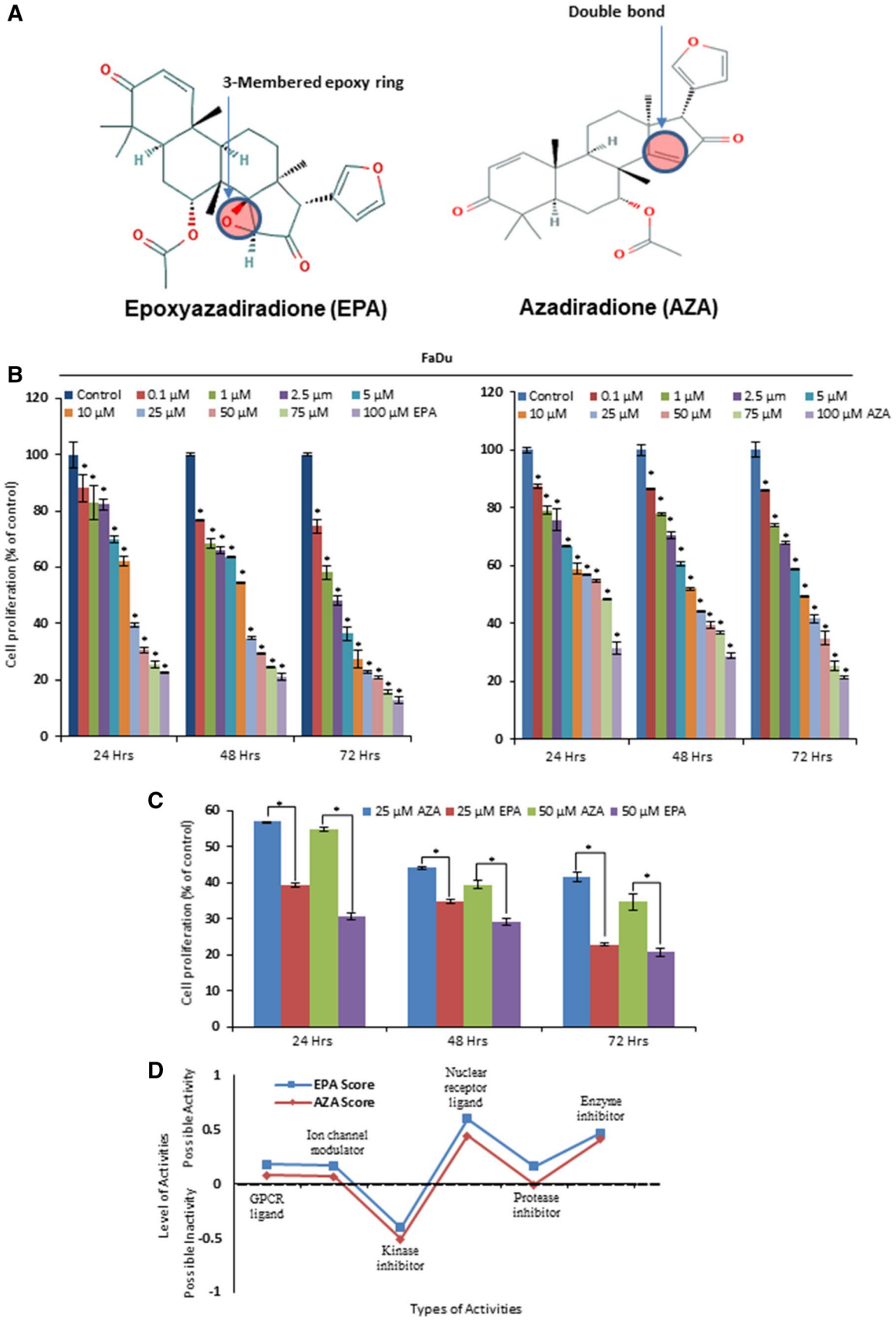
A
Double bond
3-Membered epoxy ring
Epoxyazadiradione (EPA)
Azadiradione (AZA)
B
FaDu
Control
0.1 µM
1 µM
2.5 µm
5 µM
10 µM
25 µM
50 µM
75 µM
100 µM EPA
100 µM AZA
Cell proliferation (% of control)
24 Hrs
48 Hrs
72 Hrs
C
25 µM AZA
25 µM EPA
50 µM AZA
50 µM EPA
D
EPA Score
AZA Score
Level of Activities
Possible Activity
Possible Inactivity
Ion channel modulator
Nuclear receptor ligand
Enzyme inhibitor
GPCR ligand
Kinase inhibitor
Protease inhibitor
Types of Activities

◂**Fig. 4** EPA exhibit stronger anti-proliferative activities in comparison to AZA. **a** The chemical structure of EPA and AZA. EPA contains a 3-membered epoxy ring, whereas AZA has a double bond. **b** FaDu cells were exposed to 0.1 to 100 μM EPA or AZA for 24–72 h. The anti-proliferative activity was examined by MTT assay. **c** The comparison of sensitivity of FaDu cells to 25 μM and 50 μM EPA and AZA at 24–72 h. **d** The bioactivity prediction of EPA and AZA using computational analyses. Where indicated, the values are average ± SE from 3 experiments. The significance level (*) was calculated as compared to the control group; $P < 0.05$. *EPA* epoxyazadiradione; *AZA* azadiradione

[54] activities. The current study suggests that EPA can also be repurposed for anti-carcinogenic activities.

Overall, EPA exhibited anti-cancer, anti-proliferative, pro-apoptotic, and anti-migratory activities in HNSCC lines. At the molecular level, EPA increased ROS generation, NOX-5 expression, reduced NF-κB activation, and modulated the lncRNAs expression. Further, the relative potency of EPA is stronger in comparison to AZA. To our knowledge, this is the first study evaluating EPA's efficacy against HNSCC. Future studies should delineate if the changes at the molecular level are really responsible for the anti-cancer activities of EPA. Studies are also needed to evaluate EPA's efficacy in animal models before moving for the human clinical trials.

Table 3 Drug like properties (Lipinski's rule of 5) of EPA and AZA

Parameters	EPA	AZA
logP	3.66	4.23
TPSA	86.11	73.59
Number of atoms	34	33
mol wt	466.57	450.57
Number of ON (H-bond acceptor)	6	5
Number of OHNH (H-bond donor)	0	0
Number of rotable bonds	3	3
Volume	430.17	426.11
Number of violations	0	0

AZA azadiradione; *EPA* epoxyazadiradione; *TPSA* topological polar surface area

Table 4 Predicted bioactivity score of EPA and AZA

Predicted bioactivity	EPA score	AZA score
GPCR ligand	0.18	0.08
Ion channel modulator	0.17	0.07
Kinase inhibitor	− 0.40	− 0.51
Nuclear receptor ligand	0.60	0.44
Protease inhibitor	0.16	− 0.01
Enzyme inhibitor	0.47	0.41

AZA azadiradione; *EPA* epoxyazadiradione

Table 5 In silico ADMET analysis of EPA and AZA

Absorption		Metabolism										Excretion	Toxicity	
BBB	HIA	P-Glycoprotein		CYP-450 substrate			CYP-450 inhibitor							
		Pg-S	Pg-I 1/2	2C9	2D6	3A4	1A2	2C9	2D6	2C19	3A4	ROCT	AMES	Carcinogen
EPA [**Pubchem ID:** 49863985; **SMILE ID:** CC(=O)OC1CC2C(C(=O)C=CC2(C3C1(C45C(O4)C(=O)C(C5(CC3)C)C6=COC=C6)C)C)(C)C]														
+	+	+	−/−	–	–	+	–	–	–	–	+	–	–	–
AZA [**Pubchem ID:** 12308714; **SMILE ID:** CC(=O)OC1CC2C(C(=O)C=CC2(C3C1(C4=CC(=O)C(C4(CC3)C)C5=COC=C5)C)C)(C)C]														
+	+	+	−/−	–	–	+	–	–	–	–	+	–	–	–

AZA azadiradione; *EPA* epoxyazadiradione

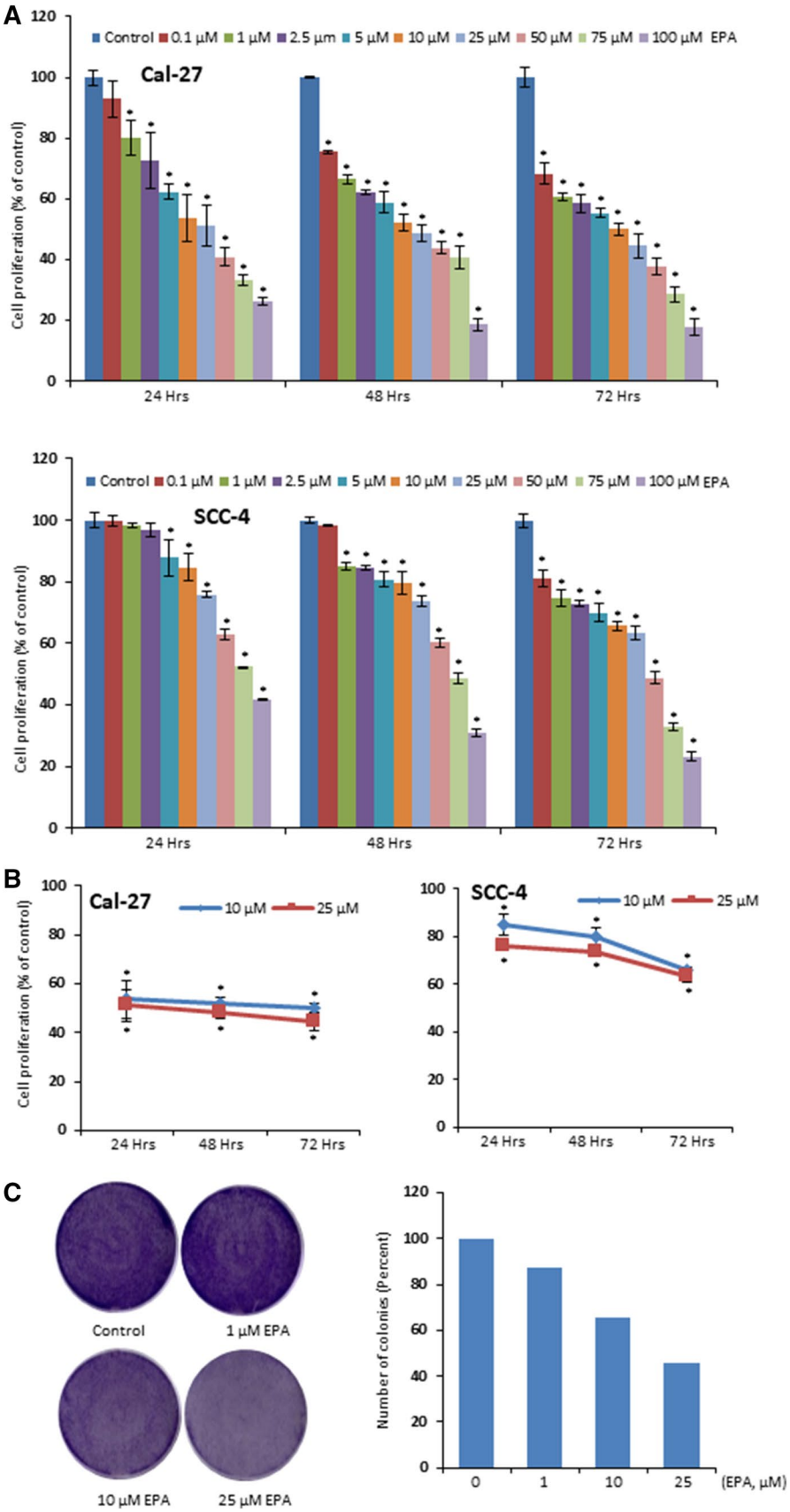

Fig. 5 EPA exhibit anti-proliferative activities in multiple HNSCC lines and reduces colony formation. HNSCC lines (Cal-27, SCC-4) were exposed to **a** 0.1–100 µM EPA for 24–72 h or **b** 10 µM and 25 µM EPA for 24–72 h. The anti-proliferative activity was determined by estimating the mitochondrial reductase activity. **c** FaDu cells were treated with 1–25 µM EPA. After 24 h, EPA was removed and the cells were left. After 10 days, the colonies were counted in a manual manner after staining with 0.1% crystal violet. Where indicated, values are average ± SE from 3 experiments. The significance level (*) was calculated as compared to the control group; $P < 0.05$. *EPA* epoxyazadiradione (Color figure online)

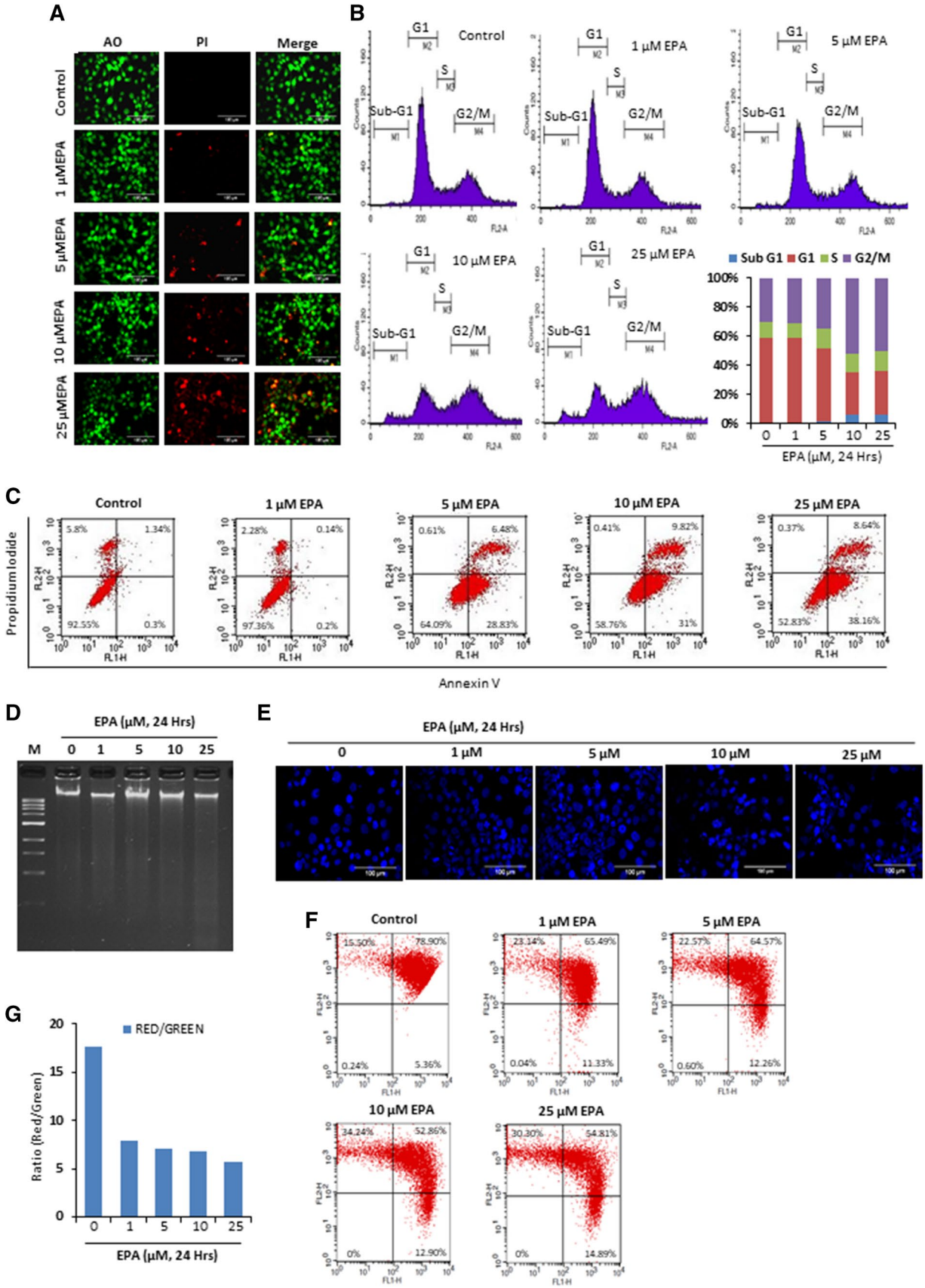
A
AO
PI
Merge
Control
1 μMEPA
5 μMEPA
10 μMEPA
25 μMEPA
B
Control
1 μM EPA
5 μM EPA
10 μM EPA
25 μM EPA
G1
S
G2/M
Sub-G1
Sub G1 G1 S G2/M
100%
80%
60%
40%
20%
0%
0 1 5 10 25
EPA (μM, 24 Hrs)
C
Control
1 μM EPA
5 μM EPA
10 μM EPA
25 μM EPA
Propidium Iodide
Annexin V
5.8%
1.34%
92.55%
0.3%
2.28%
0.14%
97.36%
0.2%
0.61%
6.48%
64.09%
28.83%
0.41%
9.82%
58.76%
31%
0.37%
8.64%
52.83%
38.16%
D
EPA (μM, 24 Hrs)
M 0 1 5 10 25
E
EPA (μM, 24 Hrs)
0 1 μM 5 μM 10 μM 25 μM
F
Control
1 μM EPA
5 μM EPA
10 μM EPA
25 μM EPA
15.50%
78.90%
0.24%
5.36%
23.14%
65.49%
0.04%
11.33%
22.57%
64.57%
0.60%
12.26%
34.24%
52.86%
0%
12.90%
30.30%
54.81%
0%
14.89%
G
RED/GREEN
Ratio (Red/Green)
20
15
10
5
0
0 1 5 10 25
EPA (μM, 24 Hrs)

◂**Fig. 6** EPA induces apoptosis through mitochondria in HNSCC lines. **a** FaDu cells were exposed to 1, 5, 10, and 25 μM EPA. After 24 h, the normal and treated cells were incubated with AO/PI and visualized under the fluorescence microscope. **b** Control and EPA exposed FaDu cells were incubated with PI, and the population in different phases of the cell cycle was analysed by flow cytometry. **c** FaDu cells were treated with 1–25 μM EPA for 24 h. The cells were then washed, stained with annexin V antibody conjugated with Alexafluor 488, and analysed by flow cytometry. **d** DNA was isolated from the normal and EPA exposed cells and electrophoresed on ethidium bromide containing 1.5% agarose gel. **e** DAPI was used to stain the cells and visualized under the fluorescence microscope. **f** FaDu cells were treated with 1–25 μM EPA for 24 h. The cells were then stained with JC-1 and analysed by flow cytometry. The upper right quadrant represents cells with JC-1 aggregates (red, heathy mitochondria) while the lower right quadrant represents cells with JC-1 monomers (green, depolarized mitochondria). **g** The ratio of intensities of JC-1 aggregates to JC-1 monomers was analysed and compared with values for control cells. *EPA* epoxyazadiradione (Color figure online)

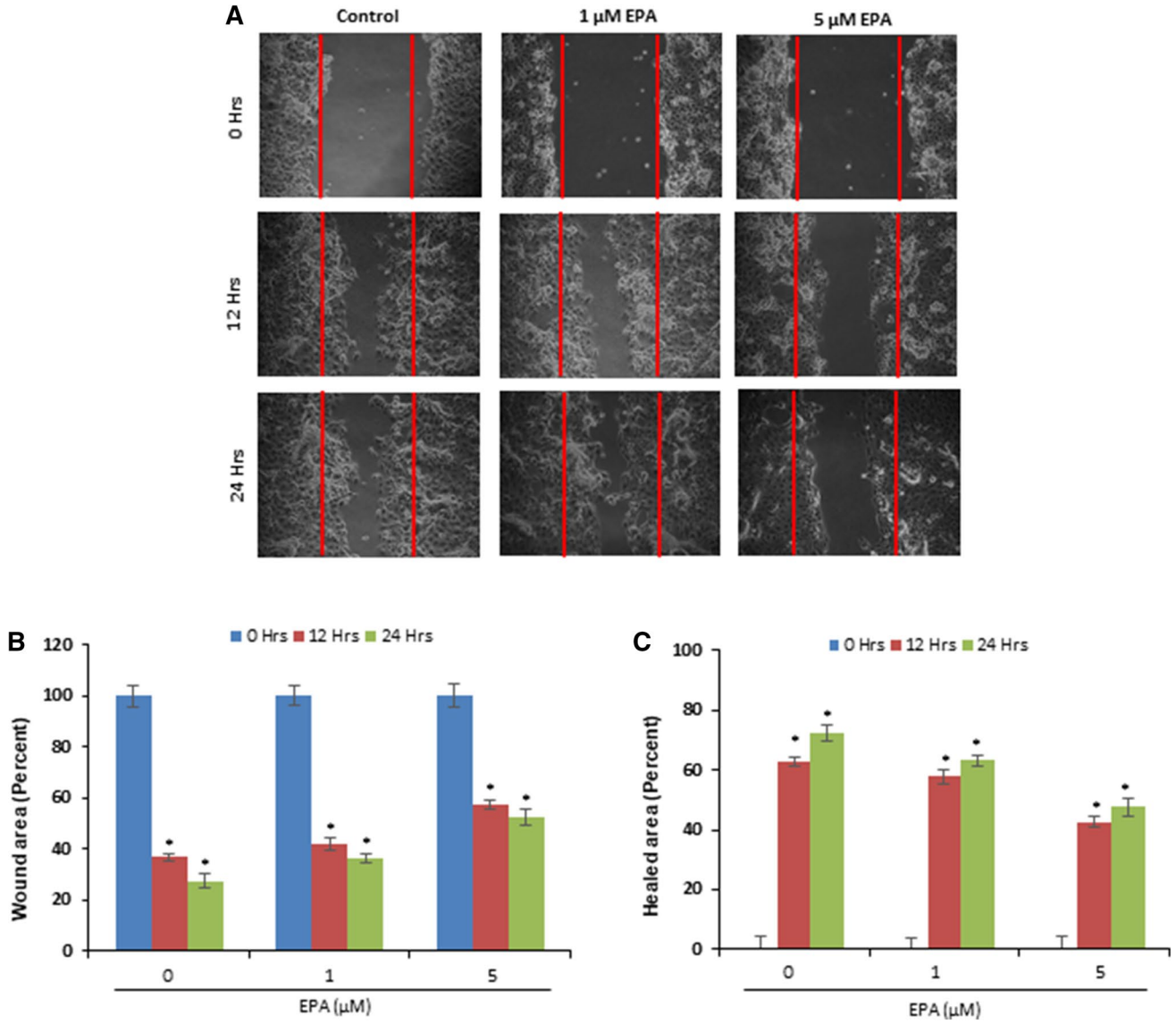

Fig. 7 EPA suppresses the migration of HNSCC lines. At 80% confluency, the monolayer of FaDu cells were scratched and cultured in media containing different concentrations of EPA. **a** The cells were visualized under the phase contrast microscope at 0 h, 12 h, and 24 h of EPA exposure. **b**, **c** The wounded area was measured over the period of treatment time. The wound size and healed area (percent) were calculated over the treatment period. Where indicated, the values are average ± SE from 3 experiments. The significance level (*) was calculated as compared to the control group; $P < 0.05$. *EPA* epoxyazadiradione

Acknowledgements The authors are thankful to Miss Anusmita Shekher for thoroughly reading the manuscript. The study was financially supported in part from Science and Engineering Research Board (Grant No. ECR/2016/000034). VR, SSV, and NA obtained fellowship from ICMR (3/2/2/43/2018/Online Onco Fship/NCD-III), DBT (DBT/2017/BHU/786) and ICMR (5/3/8/40/ITR-F/2019-ITR), respectively. We thank Dr. Rahul Kumar Singh, Department of Zoology, BHU for providing Chemi-Doc system. The support from BHU's Interdisciplinary School of Life Sciences with the microscopy, flow cytometry and real-time PCR facilities is thankfully acknowledged.

Compliance with ethical standards

Conflict of interest The authors declare that they have no conflict of interest.

References

1. Bray F, Ferlay J, Soerjomataram I, Siegel RL, Torre LA, Jemal A (2018) Global cancer statistics 2018: GLOBOCAN estimates of incidence and mortality worldwide for 36 cancers in 185 countries. CA Cancer J Clin 68:394–424

2. Poddar A, Aranha R, Royam MM, Gothandam KM, Nachimuthu R, Jayaraj R (2019) Incidence, prevalence, and mortality associated with head and neck cancer in India: protocol for a systematic review. Indian J Cancer 56:101
3. Llewellyn C, Johnson N, Warnakulasuriya K (2001) Risk factors for squamous cell carcinoma of the oral cavity in young people—a comprehensive literature review. Oral Oncol 37:401–418
4. Toner M, O'Regan E (2009) Head and neck squamous cell carcinoma in the young: a spectrum or a distinct group? Part 1. Head Neck Pathol 3:246–248
5. Greenlee RT, Hill-Harmon MB, Murray T, Thun M (2001) Cancer statistics, 2001. CA Cancer J Clin 51:15–36
6. Rades D, Huttenlocher S, Seibold ND et al (2015) Nuclear expression of p65 (RelA) in patients receiving post-operative radiotherapy for locally advanced squamous cell carcinoma of the head and neck. BMC Cancer 15:102
7. Bancroft CC, Chen Z, Yeh J et al (2002) Effects of pharmacologic antagonists of epidermal growth factor receptor, PI3K and MEK signal kinases on NF-κB and AP-1 activation and IL-8 and VEGF expression in human head and neck squamous cell carcinoma lines. Int J Cancer 99:538–548
8. Duffey DC, Chen Z, Dong G et al (1999) Expression of a dominant-negative mutant inhibitor-κBα of nuclear factor-κB in human head and neck squamous cell carcinoma inhibits survival, proinflammatory cytokine expression, and tumor growth in vivo. Cancer Res 59:3468–3474
9. Gupta SC, Kim JH, Prasad S, Aggarwal BB (2010) Regulation of survival, proliferation, invasion, angiogenesis, and metastasis of tumor cells through modulation of inflammatory pathways by nutraceuticals. Cancer Metastasis Rev 29:405–434
10. Gupta SC, Awasthee N, Rai V, Chava S, Gunda V, Challagundla KB (2019) Long non-coding RNAs and nuclear factor-B crosstalk in cancer and other human diseases. Biochim et Biophys Acta (BBA) Rev Cancer 1873:188316
11. Gupta SC, Hevia D, Patchva S, Park B, Koh W, Aggarwal BB (2012) Upsides and downsides of reactive oxygen species for cancer: the roles of reactive oxygen species in tumorigenesis, prevention, and therapy. Antioxid Redox Signal 16:1295–1322
12. Souza LC, Mishra S, Chakraborty A, Shekher A, Sharma A, Gupta SC (2020) Oxidative stress and cancer development: are noncoding RNAs the missing links? Antioxid Redox Signal. https://doi.org/10.1089/ars.2019.7987
13. Newman DJ, Cragg GM (2012) Natural products as sources of new drugs over the 30 years from 1981 to 2010. J Nat Prod 75:311–335
14. Gupta SC, Prasad S, Tyagi AK, Kunnumakkara AB, Aggarwal BB (2017) Neem (*Azadirachta indica*): an Indian traditional panacea with modern molecular basis. Phytomedicine 34:14–20
15. Gorantla NV, Das R, Chidambaram H et al (2020) Basic Limonoid modulates Chaperone-mediated Proteostasis and dissolve *Tau fibrils*. Sci Rep 10:1–19
16. Kikuchi T, Ishii K, Noto T et al (2011) Cytotoxic and apoptosis-inducing activities of limonoids from the seeds of *Azadirachta indica* (neem). J Nat Prod 74:866–870
17. Kumar D, Haldar S, Gorain M et al (2018) Epoxyazadiradione suppresses breast tumor growth through mitochondrial depolarization and caspase-dependent apoptosis by targeting PI3K/Akt pathway. BMC Cancer 18:52
18. Shilpa G, Renjitha J, Saranga R et al (2017) Epoxyazadiradione purified from the Azadirachta indica seed induced mitochondrial apoptosis and inhibition of NFκB nuclear translocation in human cervical cancer cells. Phytother Res 31:1892–1902
19. Cohen E, Quistad GB, Casida JE (1996) Cytotoxicity of nimbolide, epoxyazadiradione and other limonoids from neem insecticide. Life Sci 58:1075–1081
20. Alam A, Haldar S, Thulasiram HV et al (2012) Novel anti-inflammatory activity of epoxyazadiradione against macrophage migration inhibitory factor inhibition of tautomerase and proinflammatory activities of macrophage migration inhibitory factor. J Biol Chem 287:24844–24861
21. Gupta SC, Kannappan R, Kim J et al (2011) Bharangin, a diterpenoid quinonemethide, abolishes constitutive and inducible nuclear factor-κB (NF-κB) activation by modifying p65 on cysteine 38 residue and reducing inhibitor of nuclear factor-κB α kinase activation, leading to suppression of NF-κB-regulated gene expression and sensitization of tumor cells to chemotherapeutic agents. Mol Pharmacol 80:769–781
22. Gupta SC, Prasad S, Sethumadhavan DR, Nair MS, Mo Y-Y, Aggarwal BB (2013) Nimbolide, a limonoid triterpene, inhibits growth of human colorectal cancer xenografts by suppressing the proinflammatory microenvironment. Clin Cancer Res 19:4465–4476
23. Mishra S, Verma SS, Rai V et al (2019) Curcuma raktakanda induces apoptosis and suppresses migration in cancer cells: role of reactive oxygen species. Biomolecules 9:159
24. Herrmann M, Lorenz H, Voll R et al (1994) A rapid and simple method for the isolation of apoptotic DNA fragments. Nucleic Acids Res 22:5506
25. Verma SS, Rai V, Awasthee N et al (2019) Isodeoxyelephantopin, a sesquiterpene lactone induces ROS generation, suppresses NF-κB activation, modulates LncRNA expression and exhibit activities against breast cancer. Sci Rep 9:1–16
26. Bognar Z, Fekete K, Antus C et al (2017) Desethylamiodarone—a metabolite of amiodarone—induces apoptosis on T24 human bladder cancer cells via multiple pathways. PLoS ONE 12:e189470
27. Gupta SC, Singh R, Pochampally R, Watabe K, Mo Y-Y (2014) Acidosis promotes invasiveness of breast cancer cells through ROS-AKT-NF-κB pathway. Oncotarget 5:12070
28. Gupta SC, Singh R, Asters M et al (2016) Regulation of breast tumorigenesis through acid sensors. Oncogene 35:4102–4111
29. Awasthee N, Rai V, Verma SS, Francis KS, Nair MS, Gupta SC (2018) Anti-cancer activities of Bharangin against breast cancer: evidence for the role of NF-κB and lncRNAs. Biochim et Biophys Acta (BBA) 1862:2738–2749
30. Zhang H-j, Wei Q-f, Wang S-j et al (2017) LncRNA HOTAIR alleviates rheumatoid arthritis by targeting miR-138 and inactivating NF-κB pathway. Int Immunopharmacol 50:283–290
31. Schmittgen TD, Livak KJ (2008) Analyzing real-time PCR data by the comparative C T method. Nat Protoc 3:1101
32. Cheng F, Li W, Zhou Y et al (2012) AdmetSAR: a comprehensive source and free tool for assessment of chemical ADMET properties. ACS Publications, Washington, D.C.
33. Morris GM, Huey R, Lindstrom W et al (2009) AutoDock4 and AutoDockTools4: automated docking with selective receptor flexibility. J Comput Chem 30:2785–2791
34. Dhasmana A, Jamal QMS, Gupta R et al (2016) Titanium dioxide nanoparticles provide protection against polycyclic aromatic hydrocarbon BaP and chrysene-induced perturbation of DNA repair machinery: a computational biology approach. Biotechnol Appl Biochem 63:497–513
35. Yang N, Xiao W, Song X, Wang W, Dong X (2020) Recent advances in tumor microenvironment hydrogen peroxide-responsive materials for cancer photodynamic therapy. Nano-Micro Lett 12:15
36. Del Río LA, Corpas FJ, Sandalio LM, Palma JM, Gómez M, Barroso JB (2002) Reactive oxygen species, antioxidant systems and nitric oxide in peroxisomes. J Exp Bot 53:1255–1272
37. Jiang X, Wang J, Deng X et al (2019) Role of the tumor microenvironment in PD-L1/PD-1-mediated tumor immune escape. Mol Cancer 18:10

38. Myers JN, Greenberg JS, Mo V, Roberts D (2001) Extracapsular spread: a significant predictor of treatment failure in patients with squamous cell carcinoma of the tongue. Cancer Interdiscip Int J Am Cancer Soc 92:3030–3036
39. Gupta SC, Sundaram C, Reuter S, Aggarwal BB (2010) Inhibiting NF-κB activation by small molecules as a therapeutic strategy. Biochim et Biophys Acta (BBA) Gene Regul Mech 1799:775–787
40. Mattson M, Meffert MK (2006) Roles for NF-κB in nerve cell survival, plasticity, and disease. Cell Death Differ 13:852–860
41. Takes RP, Rinaldo A, Silver CE et al (2012) Distant metastases from head and neck squamous cell carcinoma. Part I. Basic aspects. Oral Oncol 48:775–779
42. Chaturvedi M, Sung B, Yadav V, Kannappan R, Aggarwal BB (2011) NF-κB addiction and its role in cancer:'one size does not fit all'. Oncogene 30:1615–1630
43. Yu X, Li Z (2015) Long non-coding RNA HOTAIR: a novel oncogene. Mol Med Rep 12:5611–5618
44. Özeş AR, Miller DF, Özeş ON et al (2016) NF-κB-HOTAIR axis links DNA damage response, chemoresistance and cellular senescence in ovarian cancer. Oncogene 35:5350–5361
45. Chen H, Xin Y, Zhou L et al (2014) Cisplatin and paclitaxel target significant long noncoding RNAs in laryngeal squamous cell carcinoma. Med Oncol 31:246
46. Mourtada-Maarabouni M, Pickard M, Hedge V, Farzaneh F, Williams G (2009) GAS5, a non-protein-coding RNA, controls apoptosis and is downregulated in breast cancer. Oncogene 28:195–208
47. Ke K, Sun Z, Wang Z (2018) Downregulation of long non-coding RNA GAS5 promotes cell proliferation, migration and invasion in esophageal squamous cell carcinoma. Oncol Lett 16:1801–1808
48. Guo Z, Wang Y, Zhao Y et al (2017) Genetic polymorphisms of long non-coding RNA GAS5 predict platinum-based concurrent chemoradiotherapy response in nasopharyngeal carcinoma patients. Oncotarget 8:62286
49. Yin D, He X, Zhang E, Kong R, De W, Zhang Z (2014) Long noncoding RNA GAS5 affects cell proliferation and predicts a poor prognosis in patients with colorectal cancer. Med Oncol 31:253
50. Takac P, Kello M, Vilkova M et al (2020) Antiproliferative effect of acridine chalcone is mediated by induction of oxidative stress. Biomolecules 10:345
51. Kwak A-W, Choi J-S, Liu K et al (2020) Licochalcone C induces cell cycle G1 arrest and apoptosis in human esophageal squamous carcinoma cells by activation of the ROS/MAPK signaling pathway. J Chemother 32:132–143
52. Touyz RM, Anagnostopoulou A, Rios F, Montezano AC, Camargo LL (2019) NOX5: molecular biology and pathophysiology. Exp Physiol 104:605–616
53. Siddiqui BS, Ali ST, Rajput MT, Gulzar T, Rasheed M, Mehmood R (2009) GC-based analysis of insecticidal constituents of the flowers of *Azadirachta indica* A. Juss Nat Prod Res 23:271–283
54. Thillainayagam M, Malathi K, Anbarasu A, Singh H, Bahadur R, Ramaiah S (2019) Insights on inhibition of Plasmodium falciparum plasmepsin I by novel epoxyazadiradione derivatives–molecular docking and comparative molecular field analysis. J Biomol Struct Dyn 37:3168–3182